RSC Advances

This article can be cited before page numbers have been issued, to do this please use: J. Kim and T. Lu, *RSC Adv.*, 2016, DOI: 10.1039/C5RA27080D.

ROYAL SOCIETY OF CHEMISTRY

www.rsc.org/advances

View Article Online
DOI: 10.1039/C5RA27080D

RSC Advances

PAPER

Bio-inspired Janus composite nanoscroll for on-demand tumor targeting

Jeong-Hwan Kim*[a,b] and Tsai-Ming Lu[b]

Received 00th January 20xx,
Accepted 00th January 20xx

DOI: 10.1039/x0xx00000x

www.rsc.org/

Inspired by responsive characteristics of natural fibrous counterparts, triple stimuli, pH-, drug-, and near-infrared (NIR) light-responsive Janus composite nanosheets (JCNs) are investigated. The nanosheets are consisted of gold islands sequentially hetero-grafted with three different biocompatible polymers (gum arabic, chitosan, and poly(ε-caprolactone)-b-polyethylene glycol (PEG-*b*-PCL)), which is hierarchically synthesized by a physical deposition-surface functionalization-chemical exfoliation processes. The JCNs are elastic to go through pH-controlled shape recovery activity, in a reversible manner. Remarkably, anchoring the heat-sensitive PEG-*b*-PCL on the chitosan side of JCNs, the JCNs are securely self-scrolled when doxorubicin molecules are loaded; unscrolled to release the drug under remotely NIR-irradiation, with negligible premature release, which mimic the structural behavior of a spore launcher in ferns. Moreover, the scrolled JCNs show exceptional photothermal stability under NIR-laser irradiation and the optical hyperthermal effect capable of inducing death of tumor cells, as well as bright fluorescence and a targeted photothermal anti-tumor effect under two-photon fluorescence imaging, enabling complex nano-therapeutic drug vehicle development in potential cancer theranosis with a low toxic side-effect.

1. Introduction

As a hallmark of nature's role, selective shape changing ability in response to physicochemical stimuli allows precisely tuned regulation over the favorable functional processes, mainly in plants.[1] An example is the discovery of fibrous motors in plants, which is the opening machine of seed/spore containers such as legume pods or fern sporangia to release the seeds/spores.[1c-h] The pod walls are 'Janus' 2-dimensional (2-D) structure with two distinct fibrous hydration regions.[1e,f] Dehydration of the maturing pod walls leads to a torsional kink that ruptures the pod and spread the seeds in different directions.[1e-h] The asymmetric bilayer structural model is complex and still mysterious, but extremely useful to mimic and multifunctional mimetic designs where fibers can serve both as structural elements and as responsive motors.

By taking symmetry-breaking approaches to convey different properties within a single structure, recent research focus lies on 'Janus' nanostructures,[2a,b] e.g., Janus particles, Janus cylinders, and Janus discs (platelets and sheets). Especially, the polymer-based 2-D nanosheets[2c-g] have a large surface area with extended component of different polymers reacts differently to an external stimulus, e.g., pH, temperature, or wettability, behave like a natural fibrous system. Among them, smart emulsion-based drug delivery sheet systems, which interact with intercellular stimuli, such as pH change, temperature, molecular interactions, are becoming increasingly important for controlled and triggered release of anti-cancer drugs.[2c-e] Thus, it will be attractive if the Janus interfacing-based nanosheets are responsive to the events, and the drug release can be simply manipulated on command. Ionic liquids have been devised a method for the large-scale preparation of Janus nanosheets that can form emulsions of immiscible liquids.[2c-g] Compared with colloidal stability of conventional emulsion-based drugs, e.g. micelles and liposomes, Janus nanosheets are more difficult to turn over at an emulsion interface due to their highly anisotropic (asymmetric) shape, and make an emulsion more stable.[2c-f] The underlying mechanism of the drug (seed) loading and triggered-release activities involve the entrapment of drug (seed) payloads inside the nanosheet and a stimuli-induced phase change, respectively, as natural seed dispersal systems do. This will offer us inspiration to develop advanced smart drug carrier systems, although heterogeneous nanosheet-emerged with responsive materials in this regime are rarely studied.[2c-g]

Herein, we report the efficient synthesis of smart 2D 'Janus' composite nanosheet (JCN) heterogeneous structures. The JCNs are composed of gold islands embedded in two oppositely pH-sensitive branched polymer chains (Scheme 1a). As similarly demonstrated in our previous report,[3] the rolling is not spontaneous and pH-controllable configurations because Chitosan (Chi) and gum arabic (GA) are selected as a smart polymer, which becomes expanded/shrinked at protonated states (lower pH values) and shrinks/expands at non-protonated states (higher pH values), respectively.[3]

[a] *Cardiovascular Research Institute, Yokohama City University, Graduate School of Medicine, 3-9 Fukuura, Kanazawa-ku, Yokohama,236-0004, Japan, Email: Jeongkim@yokohama-cu.ac.jp*
[b] *Nanoparticles by Design Unit, Okinawa Institute of Science and Technology, 1919-1 Tancha, Onna-Son, Okinawa, 904-0495, Japan, Email: tsaiming.lu@oist.jp*

† Electronic supplementary information (ESI) available: Additional photos of synthesis of the Janus nanosheets; additional characterization of nanosheets and drug loading; control tests of fluorescence- and two photon-imaging. See DOI: 10.1039/x0xx00000x

View Article Online
DOI: 10.1039/C5RA27080D

RSC Advances

PAPER

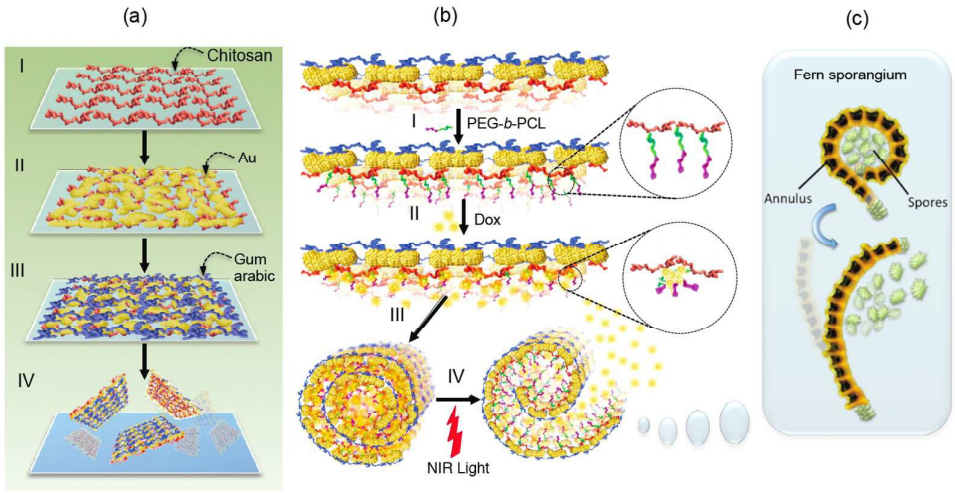

Scheme 1 (a) Illustration of sequential asymmetric preparation of Janus composite nanosheets: (I) Chitosan matrix was spin-coated onto a glass wafer, (II) Au was sputtered onto the polymer-coated surface until a near-percolating Au thin film was obtained, (III) the Au surface was functionalized with gum arabic and (IV) dipped in acetate solution and exfoliated by ultra-sonication, followed by purification and re-suspension of the nanosheets in deionized water. (b) The functionalization of PEG-*b*-PCL block copolymers on the chitosan side of nanosheet (I), Dox loading (II), triggered scrolling (III), and NIR-induced unscrolling of nanosheet resulting to the drug release (IV), (c) mimicking real spore launching system in fern sporangia.

Moreover, the thermo-sensitive PEG-*b*-PCL was linked at the Chi-layer on the JCN, enabling to control loading by a drug-to-PCL-hydrophobic interaction and releasing drug molecules by unrolling in response to NIR light-induced heating (Scheme 1b): Selective functionalization of PEG-*b*-PCL site creates JCN with a hydrophobic interior surface and a hydrophilic exterior surface, which mimicking proteins and biomembranes. Further, the shape transformations at different protonation/drug loading/photothermal states, which correspond to different pH/hydrophobicity/temperature values, were monitored by transmission electron microscopy (TEM), atomic force microscopy (AFM), UV-vis spectroscopy, and zeta-potential measurements. Specially, the drug release appears like a spore launcher in fern sporandium. (Scheme 1c). As a proof-of-concept of the efficacy of bio-inspired smart JCNs that are able to control in response to specific stimuli, either endogenous (rolling by changes in pH or hydrophobic drug molecules) or exogenous (unrolling by heating via NIR light), we assessed NIR-guided in vitro photothermal treatments of JCNs on HeLa cells.

2. Experimental Section

2.1. Synthesis of the JCNs

All reactions were performed under an atmosphere of nitrogen, and all chemicals were of analytical grade and used without further purification. A ultrapure deionized (DI) water was used from a MilliQ system (Nihon Millipore K.K., Tokyo, Japan) using 0.1 µm filters. A 2" glass wafer was thoroughly ultrasonicated in dry methanol for 10 min and dried with N_2 gas. A thin polymer film was formed by spin-coating 20 mg of Chi (Sigma-Aldrich, St. Louis, US) that had been dissolved in 500 µL of 1% (v/v) acetic acid solution, and gently dispensed onto the cleaned glass substrate at 3,000 rpm or 30 sec (MS-A-150 spin-coater, Mikasa, Japan). Au nanostructures were deposited by magnetron sputtering of a 2" Au target (99.99%) (Ted Pella, Inc., Redding, CA, US) onto the Chi-coated substrate for 60 sec at a DC power of 4 W until a near-percolating thin film was obtained by a modification of our previous method.[3] The samples were gently immersed in a DI water solution of 20 mg/mL GA (Sigma-Aldrich, St. Louis, US) and incubated for 60 min and washed with DI water three times and re-immersed in 1% acetic acid solution to dissolve the Chi-layer, followed by an ultrasonication at 20 kHz for 15 min at 20 W with a Hone T-01 ø3.9 mm sonication tip attached to an ultrasonic homogenizer (Model 150 V/T, BioLogics Inc., Manassas, Virginia, US). This was followed by mild agitation for 30 min, and a separation step to remove excessive Chi polymers using a centrifuge at 3,000 rpm for 15 min. After washing with DI water, the collected JCNs were re-dispersed in DI water.

2.2. PEG-*b*-PCL Functionalization on the JCNs

View Article Online
DOI: 10.1039/C5RA27080D

To functionalize hydroxyl group of PEG-*b*-PCL (Sigma-Aldrich, St. Louis, US) onto the amine-terminated Chi moieties on the immobilized Au nanosheets, the modified method in the literature[4] was performed, as shown in Scheme 2. In order to reduce non-specific cross-linking between the surface molecules, the order of surface treatment was gum arabic, Au, and chitosan, by taking slightly modified steps in section 2.1. Briefly, GA was spin-coated onto a glass wafer, and then Au was sputtered onto the GA-coated surface, followed by the functionalizion of Chi in dichloromethane (DCM)/w 1% TFA for 1 h. After washing and drying, the JCN sample was immersed in pyridine solution. Subsequently adding 5 mM of terephthaloyl chloride (TC), the immersion lasted for 2 h under N_2 purge at room temperature and removed any excess free TC. The conjugation of TC was monitored by UV-vis spectroscopy. Then, 5 mM of PEG-*b*-PCL in pyridine was added and the reaction continued at 45 °C under nitrogen purge for 2 h. After removal of excess PEG-*b*-PCL by rinsing with pyridine, blowing with N_2, and then exfoliated by adding PBS buffer (10 mM, pH 7). The PEG-*b*-PCL polymer conjugated JCNs was evaluated by zeta potential and FTIR analysis.

2.3. Characterization of the JCNs

The size and morphology of JCNs were obtaining using JEOL JEM-1230R transmission electron microscope (TEM) at 100 keV with an accelerating voltage of 40-100kV. A MultiMode AFM (Bruker, CA) was used to acquire the AFM data in tapping mode. The optical absorbance spectra were measured using a Multiskan GO UV-visible spectrophotometer (Thermo Scientific, USA). Zeta-potential measurements were performed using a Zetasizer Nano ZSP (Malvern Instruments Ltd, Worcestershire, UK). FTIR spectra were acquired using a Bruker Vertex 80v FTIR instrument with a PIKE MIRacle™ ATR unit equipped with a ZnSe crystal. 1 mg was used to attain each spectrum. Data was achieved and analyzed using OPUS software with a scan from 400 to 4000 wavenumbers at 2 cm^{-1} resolution at 60 scans per spectrum. Both the optical bench and sample chamber were under vacuum (2-5 hPa) for each measurement to eliminate OH and CO stretching modes from H_2O vapor and CO_2 in the atmosphere.

2.4. Cell culture and viability assay

HeLa cells were incubated in were maintained in Dulbecco's modified Eagle's medium (DMEM)(Thermo, SH30021.01), supplemented with 10% fetal bovine serum (FBS)(Thermo, SH30910.03) and antibiotics (10,000 mg/mL streptomycin and 10,000 unit/mL penicillin) at 37°C in a humidified atmosphere containing 5% CO_2 (v/v). Subculturing was performed every three days and 2.2×10^6 cells were seeded on the 10 cm petri dish. The culture media were replaced with fresh media and cultured for a further 48 h. After dispensing 100 µl of cell suspension (5000 cells/well) in a 96-well plate, the plate was pre-incubated for 24 h in a humidified incubator. Then 20 µL of methyl thiazolyl tetrazolium (MTT) solution (Dojindo Cell Counting Kit-8, Japan) was added to each well and incubated for another 4 h at 37°C. After that, the absorbance at 450 nm was measured with a Multiskan GO UV-visible spectrophotometer. The viability of treated cell wells was acquired as a percentage of the viability of unexposed wells.

2.5. Photothermal properties and stability of JCN products

The plasmonic photothermal effect of LSPR feature on the Au products was investigated by near infrared (NIR) diode laser system (IR-800) (custom-made by New Vision Inc., Taiwan, http://www.nvi-laser.com/) with wavelength at 800 nm fiber-coupled to one single external fiber connected to a hand piece. The laser diode was set 0.5 cm above the liquid surface and, upon the application of NIR-laser irradiation. 0.15-0.5 W laser power on a continuous wave mode was used to irradiate either the HeLa cells in the absence or presence of JCNs in 10 mM PBS buffer. The heat sensing was performed with a thermocouple microprobe in a hyperthermia instrument DM-100 (nB nanoScale Biomagnetics, Zaragoza, Spain), submerged in the solution in a 1-cm^2 cuvette. The probe was located at such a position that the direct irradiation of the laser on the probe was evaded. After staining with LIVE/DEAD Cytotoxicity Kit for mammalian cells (L-3224, Life Technologies) for 5 min, microscopic images of the cells were obtained using a Zeiss LSM 510 multiphoton confocal microscope system through a 40X objective lens.

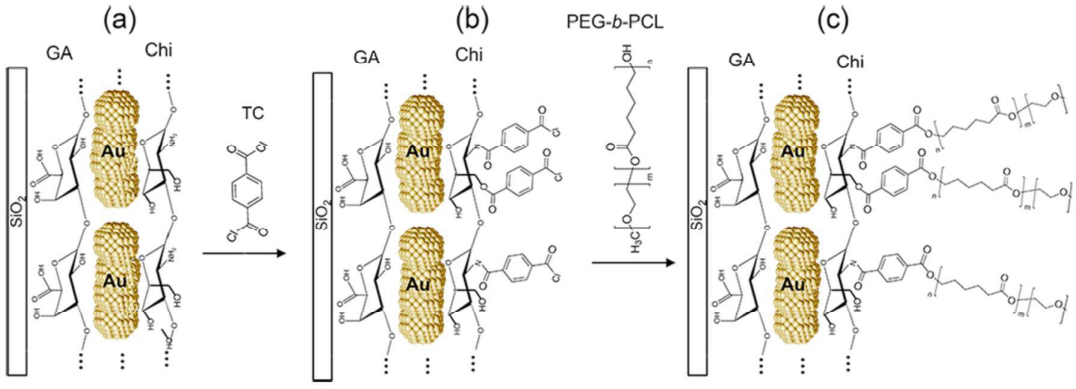

Scheme 2 Solid phase sequential bifunctionalization of JCN surface: Deposition of gum arabic, Au, and chitosan on a glass substrate (a); Linking terephthaloyl chloride (TC) with chitosan (b), and PCL-*b*-PEG polymers (c).

View Article Online
DOI: 10.1039/C5RA27080D

RSC Advances

PAPER

2.6. Single Photon/Two Photon Confocal Laser Scanning Microscopy Imaging of JCNs

The fluorescence images of JCN in the absence/presence of HeLa cell samples were captured by Zeiss LSM 510 multiphoton confocal microscope system through a 100X/40X objective lens, and 488 nm (single photon mode) and 800 nm (two photon mode) lasers were used to excite the JCNs at 37°C. HeLa cells were seeded at an initial density of 2 X 10^4 cells/well in 12-well culture plate over glass coverslips. After 24 h incubation in 5% CO_2 humidified incubator, cells were incubated with JCN samples in culture media for 2 hours.

2.7. Drug-Loading Capacity and Triggered-Release Behavior of JCNs

A solution of Dox in THF (0.04 mL, 0.25 mg/mL) was added into a suspension of JCNs in 1 mL PBS buffer solution (0.1 mg/mL). The reaction mixture was then stirred at 30°C for 1 h followed by centrifugation at 4,000 rpm for 5 min and washing three times with PBS buffer, and the resulting pellet was dried under vacuum. The as-acquired precipitated JCN pellet was dispersed in PBS buffer under sonication for 30 s in an ice-water bath and then purified by centrifugation three times (3000 rpm, 5 min) to remove the free Dox molecules. Finally, Dox-loaded JCNs were re-dispersed in PBS buffer solution under sonication for 10 s in an ice-water bath. The centrifugation supernatants were collected to estimate the loading of Dox from its UV-Vis absorbance at 495 nm by using a pre-determined calibration curve. The drug-loading capacity was determined as $(M_{initialDox} - M_{Dox\ in\ excess})/(M_{JCN})$ (mg/g), where $M_{initialDox}$ is the initial mass of Dox added, $M_{Dox\ in\ excess}$ is the mass of Dox in the supernatant, and M_{JCN} is the mass of JCN samples. The release activity of the Dox-loaded JCNs was also monitored by UV-Vis absorbance at 495 nm at different temperatures over time. At each pre-determined interval, the sample was centrifuged and its UV/Vis absorbance at 495 nm was used to quantify the amount of released Dox from the supernatant, according to a pre-determined calibration curve. All of the release profiles were shown in cumulative mode. The light-induced heating of an aqueous JCN suspension of under NIR-laser irradiation was performed by using the aforementioned laser diode (800 nm) with output power of 0.15-0.5 W.

3. Results and Discussion

3.1. Preparation of hybrid organic and inorganic Janus nanosheets

In order to synthesize the JCNs, processes of physical deposition, chemical exfoliation, and surface adsorption were involved, as resented in Scheme 1a, I-IV and Fig. S1 (Photos, ESI†). Au was sputtered onto a Chi-coated Si substrate until a near-percolating Au thin film was obtained (Scheme 1a, I-II). The Au nucleation and growth into percolating nanodomains evolved as a function of deposition time, as investigated in our previous report.[3] The other side of Au layer was functionalized with GA that correspond to JCNs (Scheme 1a, III), and exfoliated into acidic medium, followed by ultrasonication (Scheme 1a, IV), and the suspension was purified to remove the unbound polymer chains. Finally, the collected JCNs were re-suspended in deionized water. The sequence of functionalization steps is important to create the Janus heterogeneous interface. In the first step the Chi polymer chains connecting multiple domains (analogous to inner pod wall) and GA chains adsorbed only onto the outer surface of Au nanodomains (outer pod wall) are formed. Post-exfoliation, polymer chains adsorbed selectively onto the upper and outer surface of the Au nanodomain.

3.2. Structural characterization of Janus nanosheets

In TEM analysis, the JCNs laying flat on the TEM grid indicating the 2D nature of the JCNs (Fig. 1a) with near-percolating Au networks (Fig. 1b). To measure the thickness, the JCNs were dispersed on a silicon substrate and scanned in tapping mode AFM (Fig. 1c). The associated cross sectional height profiles are shown in Fig. 1d, showing that the average thickness of the JCNs was determined to be ~7 nm. It is worth noting that the stepwise coating of two different polymers with different solubility allows the heterogeneous compartmentalization of the JCNs. This is because one layer of branched polymer has been adsorbed onto the Au nanodomains, there can be no further interaction with incoming polymer layer, confirming the validity of the solid phase hetero-functionalization method used to prepare the stable JCNs. The correspondent TEM analysis of nanoscrolls is also presented in Fig. 1e,f. On the AFM image and associated cross-sectional height profile (Fig. 1g,h), the nanoscroll's layer thicknesses in (h) are nearly consistent with flat nanosheets of (d). Furthermore, the height of the scroll is proportional to the number of scrolling turns (h), showing a "one-sided scroll" architecture.

3.3. pH-responsive characterization of Janus nanosheets

View Article Online
DOI: 10.1039/C5RA27080D

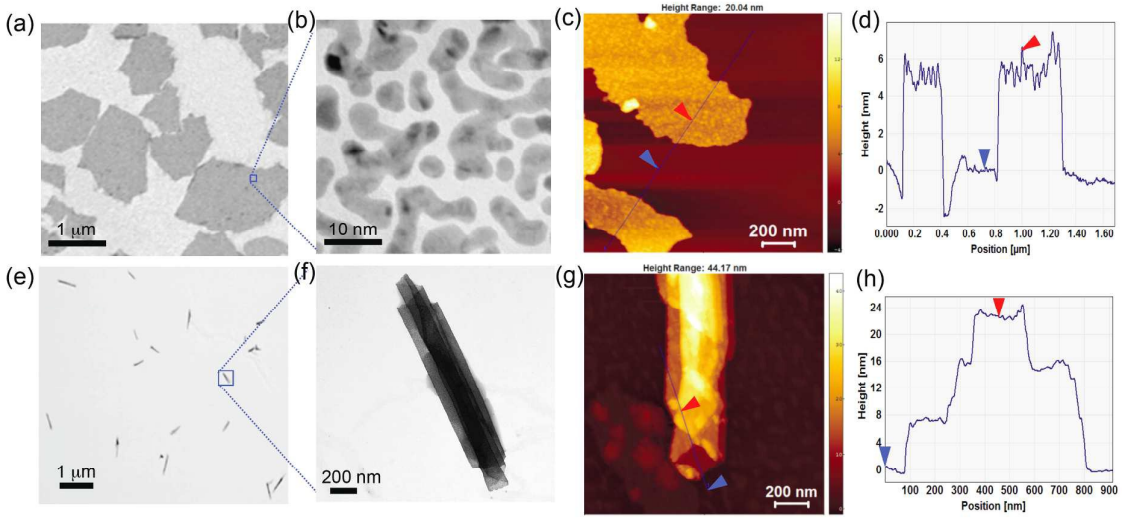

Fig. 1 TEM and AFM characterization of nanosheets in response to pH 6 (a-d) and pH 10 (e-h). TEM image of exfoliated nanosheets (a), a magnified Au nanostructures (b), and an AFM topography image of the nanosheets (c) with a cross-sectional height profile showing the thickness of a nanosheet ~7 nm (d). The correspondent TEM and AFM analysis of nanoscrolls are also shown at e-h, associated cross-sectional height profile showing that the height of the scroll is proportional to the number of unidirectional turns (h).

The 2D-JCNs show a pH-responsive shape transformation to nanoscrolls upon changing the pH value to 10, as similar as bPEI-based nanosheets in our previous report.[3] This transformation, from the initially flat JCNs at pH=6 (Fig. 1a and Fig. 2a, I) to nanoscrolls at pH=10 (Fig. 1e and Fig. 2a, II) and back to flat JCNs at pH=5 (Fig. S2 and Fig. 2a, III). The shape transformation between nanoscrolls and nanosheets was examined by UV-vis spectroscopy and zeta-potential measurements, as similar way to our earlier study.[3] The absorbance spectra were obtained for JCN at several pH values (Fig. 2b). As the pH value was increased, the absorbance spectrachanged from a spectrum typical of a thin film (2D-JCN), with a flat shoulder at long wavelengths to a spectrum typical of a metallic 1D nanostructure (nanoscroll) with a peak corresponding to the surface plasmon resonance of Au and a decreasing absorbance at longer wavelengths. Our strategy for enhancing the anti-tumor efficacy of JCNs involved the functionalization of a thermo-responsive polymer, PCL-*b*-PEG, onto the Chi surface of JCNs in order to load the JCNs with doxorubicin (Dox), a model water-insoluble chemotherapeutic agent that can be released upon NIR laser irradiation. To ensure the anchoring of PEG-*b*-PCL entities on Chi site of JCNs, we performed an UV-vis spectroscopy of acyl chloride linker moieties as shown in supporting information (Fig S3, ESI†). The subsequent UV-vis peak signature of TC was presented in the range of 200-300 nm, exhibiting ~90% grafting efficiency of acyl chloride on the chitosan layer (amine and hydroxyl moieties) on the JCNs. Furthermore, the UV-vis spectrum of PEG-*b*-PCL-conjugated JCNs can be shown in Fig. S4 (ESI†), exhibiting a new peak derived from PEG-*b*-PCL at ~280 nm, compared to that of TC-grafted JCN. Considering cross-linking can occur between Chi moieties in the presence of bifunctional linker, e.g. TC, usually in solution phase functionalization, the use of sequential solid-phase synthesis by a flat solid masking support (SiO_2), allows greater linking selectivity and ease in the bifunctionalization of TC.

The FTIR spectrum of the GA-Au-Chi nanosheets (Fig. 2c) displays not only the characteristic peaks of the original Chi at around 1080, 1620, 2900 and 3450 cm^{-1}, but also the characteristic bands of the GA at 1500–1600 cm^{-1}, confirming effective bi-modification of the nanosheets. Comparing with the GA-Au-Chi nanosheets, the FTIR spectrum of GA-Au-Chi-PCL-PEG shows the decreased peak from free Chi at 1014 cm^{-1} and the new peaks from free PEG-*b*-PCL at 982-1180 cm^{-1} and 1724 cm^{-1}, shown in Fig. S6 (ESI†), verifying that the PEG-*b*-PCL was successfully functionalized onto amine-residues on Chi surfaces. After the PEG-*b*-PCL polymer anchoring, the surface of the JCNs changed from positively charged (z=4.3 mV, pH 6.0) to almost neutral (z=1.2 mV, pH 6.0), representing the PEG-*b*-PCL was successfully grafted on the Chi-layer of JCN surface (Fig. 2d). The pH-responsive reversible shape transition of the hybrid JCN products has been further confirmed by zeta potential analyses in different pH conditions (Fig. 2d). The nearly neutral potentials indicate that the structures are stable over a wide range of pH values from 3~10, and confirm that the two differently charged polymers is strongly adsorbed onto the Au nanodomains in a balanced manner. The zeta-potential decreases as the JCN transitions to the nanoscroll, indicating a decrease in positively charged Chi-layer area consistent with rolling, while the JCN exhibited slightly faster rolling and unrolling than the bPEI-nanosheets in our previous study (Fig. S7, ESI†).

Natural polymers, e.g. polysaccharides, containing carboxyl groups or amino groups respond to the pH changes by changing their volume in the protonation/swollen state.[5] At low pH values, cationic polymers containing amino groups exhibit a stronger ionization and hence higher swelling. On the contrary, the carboxyl containing anionic polymers show minimum ionization and hence reduced hydration. As illustrated in Fig. 2a, when the pH above the pK_a of the chitosan (~6.5),[5a,5b] the amino groups start to get deprotonated, leading to polymer shrinking and "one-sided scrolling" of JCNs (I, II); At the pH below the pK_a, the amino groups

View Article Online
DOI: 10.1039/C5RA27080D

RSC Advances

PAPER

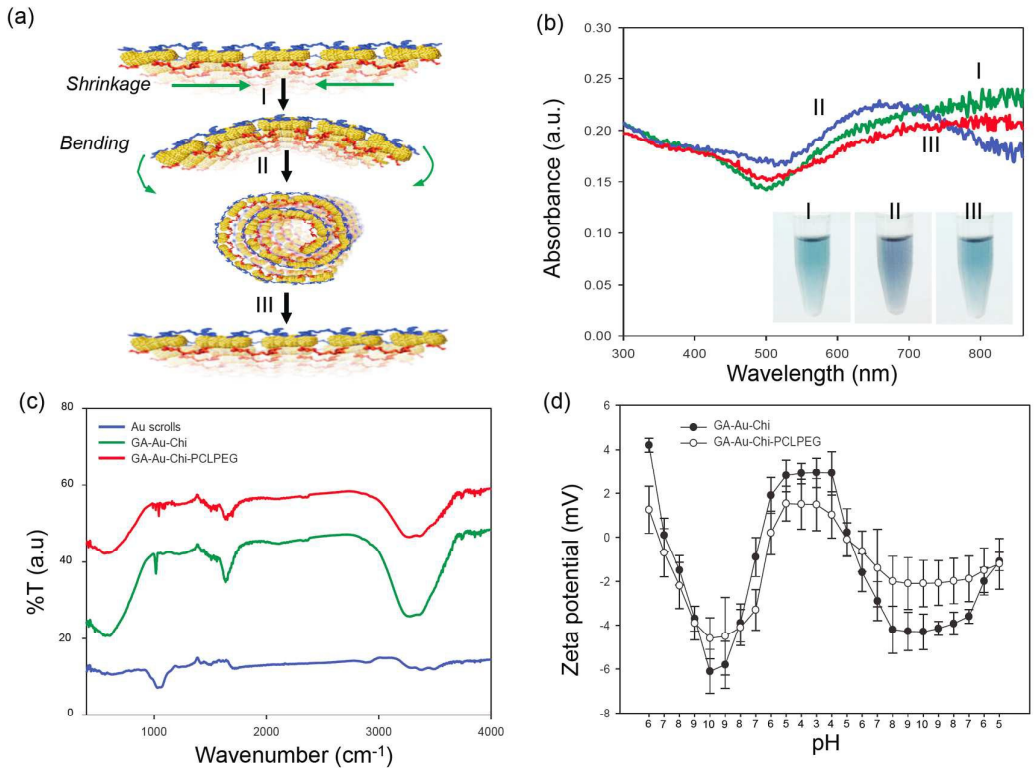

Fig. 2 (a) The scheme of pH-responsive shape-morphing of a nanosheet into a nanoscroll at alkaline pH (I, II) and unscrolling at acidic pH (III). (b) Optical absorbance spectra of GA-Au-Chi JCNs at pH's of 6 (green), 10 (blue), and 3 (red), showing pH-dependent reversible transition from flat shoulder at long-wavelengths at pH 6 (flat JCN) to peak consistent with Au plasmon resonance of 1D metallic structure for pH 10 (nanoscrolled JCN). The correspondent colors of JCN dispersions are shown with pH change (I-III). (c) FTIR spectra of Au nanoscrolls (blue), GA-Au-Chi nanosheets (green), and modified GA-Au-Chi with PEG-*b*-PCL copolymers (red). (d) Zeta-potentials indicative of the surface morphing of JCN (black circle) and modified GA-Au-Chi with PEG-*b*-PCL copolymers (white circle) at all protonation states corresponding to pH's in the range 3-10.

are protonated, which results in polymer expansion/swelling and hence unrolling of JCNs (III). However, because the pK_a of GA (~2)[5c] is relatively low, it is assumed that the electrical charge on the GA chains on the JCNs seems not so much responsible for shrinking and scrolling. Instead, at pH<3, the carboxyl groups may start to deprotonated, which results in polymer expansion and hence facilitated unrolling of JCNs synergistic with deprotonated Chi. Thus, increasing the pK_a of GA by its chemical modification would be further optimized to enhance the pH sensitivity.

3.4. Photothermal activity of Janus nanosheets

Photothermal agents with NIR absorbance properties (e.g. Au nanorods) are clinically desired for phototherm ablation (PTA) therapy due to their high tissue-penetrating capability and photothermal conversion efficiency.[6] To evaluate the PTA performance of JCNs, the photothermal properties of JCN products in two different power range of 0.15 W and 0.5 W were examined by a thermo-measurement system (Fig. 3a). We preset our initial solution temperature about 35 °C in a JCN scroll solution, assuming that most of the cancer cells will be killed when its temperature reaches about 45 °C. The substantial heat was generated linearly within a minute when excited by the NIR light (where light penetration in deep tissue is optimal). The photothermal stability of JCN products was also investigated by UV-vis spectroscopy (Fig. S8, ESI†) and TEM analysis (Fig. S9, ESI†). Interestingly, the LSPR spectra of the nanoscrolls (30 μg/mL) remained almost unaffected with slight broadening after 15 min laser irradiation (800 nm, 1 W power), in contrast, the absorption spectra of JCN sheets (30

View Article Online
DOI: 10.1039/C5RA27080D

μg/mL) were substantially broadened and blue-shifted towards shorter wavelength. Accordingly, TEM images showed that many of thin nanosheet structures were thermally damaged or buckled by the long-term laser irradiation (Fig. S9b, ESI†), whereas scrolled structures were protected by the trimly rolled multiple layers of JCN scrolls (Fig. S9d, ESI†). However, these JCN scroll colloids have a superior stability over the laser irradiation, compared to the fact that conventional anisotropic nanostructures, e.g., gold nanorods (AuNRs), are dramatically melted within 5 minutes by even lower power laser at < 0.1 W/cm^2.[7]

Next, we assessed *in vitro* PTA capacity of JCN scrolls with HeLa cells. The MTT assays presented that tumor cells treated with JCN scrolls without laser irradiation remain more than 90% viable at JCN scrolls concentrations up to 100 μg/mL (Fig. 3b), suggesting that JCN scrolls retain low cell cytotoxicity. The cell viability considerably declined when they were simultaneously treated with JCN scrolls and laser irradiation. Only about 15% of HeLa cells remained viable at a JCN scrolls concentration of >100 μg/mL, while showing a concentration-dependent photothermal ablation activity as observed by a confocal microscopic imaging (Fig. 3c).

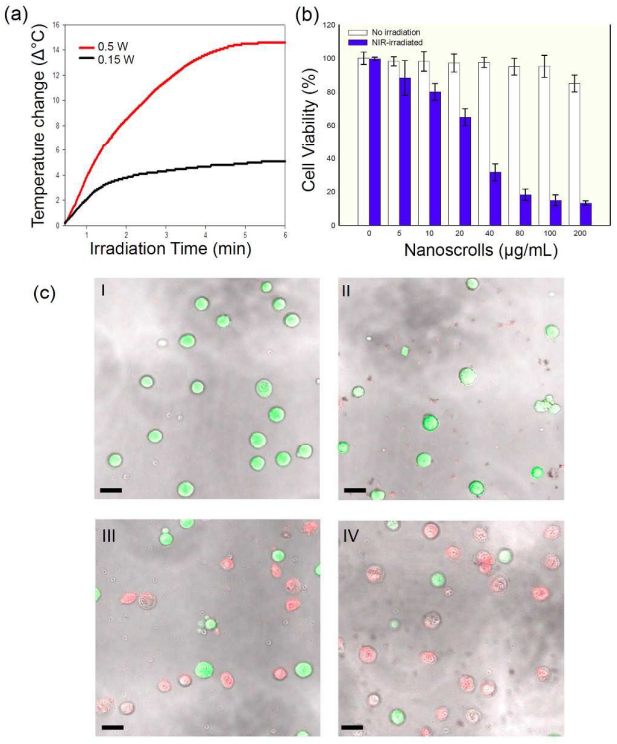

Fig. 3 Plasmonic hyperthermal effects of nanoscrolls on the laser irradiation at 0.5 W (red) and at 0.15 W (black) (a). Photothermal *in-vitro* cytotoxicity of nanoscrolls by incubating with HeLa cells (b) (error bars correspond to mean ± standard deviations). The confocal fluorescence images (c), showing HeLa cells only (I), the cells with nanoscrolls (II), the laser-irradiated cells with nanoscrolls at a low (III) and high (IV) concentration (5 and 30 μg/mL, correspondingly). Scale bar: 30 μm.

3.5. Drug loading/releasing performance of Janus nanosheets

Dox was successfully loaded and trapped within the PCL domain by the hydrophobic interaction between Dox molecules and PCL domain of PEG-*b*-PCL (Fig. 4a,c), which leading to overall JCN layer (Chi-site) to be hydrophobic, hence results to scrolling, as a similar fashion of a micelle formation in aqueous medium. The drug-loading capacity (DLC) was determined spectrophotometrically (Fig. S5, S6) to be about 42.4 wt%, with a drug-loading efficiency (DLE) of about 93.3 wt%. This relatively high DLC, compared with DLCs of up to 22.6 wt% as studied elsewhere[8] could be attributed to the high PCL polymer fraction along the large surface area of JCN structure. Heat-induced phase-change of PCL site influenced the temperature-dependent optical properties of JCN under heating. In relation to the triggered-release behaviour by conventional external heating, the release of Dox was reserved at 25 °C and 37 °C. Conversely, sustainable release was found during the subsequent release at 37 °C after activation at 50 °C for 30 min. The heat-triggered release mechanism is assumed to be associated with the melting of the PCL crystallites, which resulted in enhanced permeability of the amorphous PCL domains and a higher diffusion coefficient of the Dox molecules. The JCNs after Dox-loading and NIR-induced releasing were morphologically evaluated by TEM imaging (Fig. 4a,b), showing scrolled and unscrolled feature, respectively (Fig. 4c, inset: no noticeable fluorescence of Dox upon loading into the JCNs, while it may be possibly self-quenched at the high density state encapsulated inside the scrolls). The JCN solution after Dox releasing showed the UV-absorption curves at 290-320 nm from PEG-PCL/Chi residues and the elevated NIR curve at 750-900 nm (Fig. 4c), while Dox molecules in supernatant solution of the sample are fluorescing after separation (Fig. 4c, inset: Dox emits light upon release into the surrounding buffer), representing that the Dox molecules were released during the nanoscrolls were unscrolled. Based on the drug release profile (Fig. 5a,b), high Dox (70%) release was observed in water-heating at 50°C for 30 min and remained at 37°C for 47.5 h induced release, observed as a large increase in UV-vis intensity at 475 nm, whereas low Dox (5%) release occurs at neutral pH (pH 7.4) within 48 h, indicating that they could act as a drug delivery system with the possibility of delivering water-insoluble drug payloads with minimal premature release, whilst a remarkable remotely triggered release of drug payloads may occur under NIR irradiation. On the other hand, the presence of JCNs opened up the application of NIR light as a remote stimulus to trigger the release upon NIR-laser irradiation for 30 min (800 nm), with only mild heating (<48°C) of the overall release medium, thus promising less side-effects on the tissue surroundings. Cytotoxicity tests of Dox-loaded JCNs against the HeLa cell-line also revealed outstanding compatibility with improved anticancer activity (~4% of HeLa cells remained viable at a JCN scrolls concentration of >100 μg/mL) (Fig. 5c). The scrolling and loading drug molecules activities of JCN inner wall is a bit similar to annulus cells in fern sporangia, consisted with a row of cells that enclosing the spores by rolling one side; The hydration of JCN inner wall side is dominant to the Dox ejection process, reversely to the spore launching annulus system: As the annulus cells dehydrated, increased water tension inside the cell triggers lateral walls to collapsible internally, followed by bending the walls and discharging the spores.[1h]

View Article Online
DOI: 10.1039/C5RA27080D

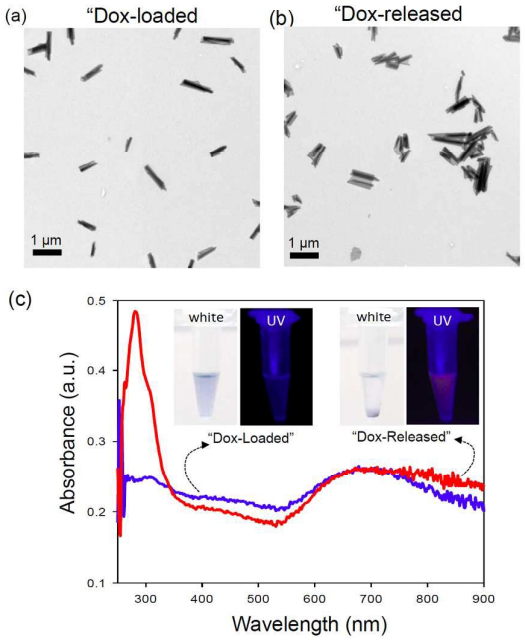

Fig. 4 TEM images of nanoscrolls loaded with Dox before release (a) and after release by NIR-irradiation (b). UV-vis absorption spectra of the corresponding Dox-loaded (blue) and released (red) nanosheet solutions after separation (c) (The related sample photographs are shown in the inset: The Dox-loaded nanoscrolls are shown blue color under white light, while Dox molecules in supernatant solution of the sample (after centrifuged) are fluorescing under UV light.

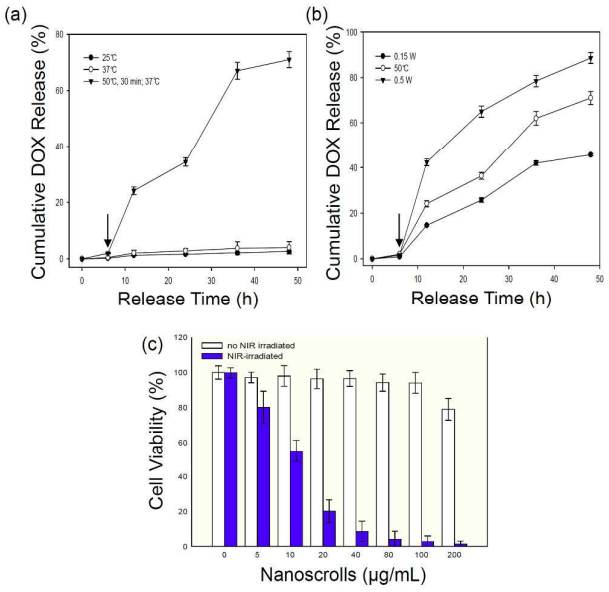

Fig. 5 Release profiles of Dox from a Dox-loaded JCN suspension at different heating modes (a,b): The release at 50°C after water heating was performed as follows (a): An initial release for 6 h at 37°C to mimic the *in vivo* delivery routine, then heating for 30 min at 50°C to emulate the heat treatment (marked with an arrow), and finally release for 42 h at 37°C to imitate the release under physiological conditions after the treatment. The bar graphs represent the mean values (standard deviation) from three independent experiments. The release over 42 h at 37°C after NIR laser irradiation for 30 min (800 nm, 0.15 or 0.5 W, marked with an arrow) (b); the release behaviour at 37°C after heating at 50°C for 30 min was also noted for comparison. Photothermal *in-vitro* cytotoxicity of Dox-loaded nanoscrolls by incubating with HeLa cells (c) (error bars correspond to mean ± standard deviations).

PCL is a biodegradable, hydrophobic, linear, aliphatic, and thermo-responsive polyester, which has been widely used in the therapeutic biomedical field for the last few decades.[9] However, the realization of therapeutic micelle systems is still limited due to low loading efficiency, leak/burst release, and low bioactivity.[9a] Alternatively, on the basis of PCL-PEG-based micelle design, pH-triggered charge reversal system has been studied, particularly for intracellular drug delivery.[9b] Consequently, JCN design could challenge the limited utility of PCL-based heat- and pH-responsive drug carriers. Furthermore, although the loading and release efficiency of current JCN design are relatively lower than commercial products such as Doxil® or Doxoves®, the structurally responsive, stable, and high surface area-based formulation design in "minimally-invasive" and "on-demand" hydrophobic drug delivery may counterbalance the JCN's drawback by further optimization in the future.

3.6. Two-photon fluorescence imaging of Janus nanosheets

In addition, JCNs exhibited higher brightness under two-photon excitation than one-photon excitation as shown in Fig. 6, which may possess fluorescence property in the NIR region due to the high light absorption coefficient and ability to sustain resonating localized surface plasmons with minimal damping, as analogous as Au nanorods.[10] Especially, two-photon microscopy is less damaging to thin optical sections of the nanosheets with improved resolution along the z dimension than the single-photon confocal microscopy (Fig. 6b,c). In the meantime, folded nanosheets and nanoscrolls (Fig. 6b,c) exhibited significantly brighter intensity compared with flat nanosheets (Fig. 6e,f) as well as the spherical Au nanoparticles (~15 nm), showing nearly no fluorescence (Fig. S10, ESI†), which is presumed when the hybrid nanoscrolls' are folded/rolled, many 'hot spots' can be formed along the multi-layers producing a larger electromagnetic field enhancement and a great increase in the fluorescence intensity on the JNS surface, in which overall localized SPR were amplified at the NIR region. The advantage of fluorescence in NIR region is that it allows the use of light in the tissue transparent window (700-1000 nm) enabling deeper penetration of NIR light and minimized risk of laser hyperthermia.

3.7. Two-photon-induced photothermal cancer imaging and targeting by Janus nanosheets

Henceforth, we investigated the TP-induced photothermal activity of the JCNs on the HeLa cells are shown in Fig. 7. Comparing to the high irradiation level with the fiber-optic laser power (0.5 W), most of the cells can be killed in the presence of JCNs after several scans (30 min) at an extremely low laser power of 0.1 mW (Fig. 7b), while no cell death was observed in the absence of JCNs (Fig. S11, ESI†).

View Article Online
DOI: 10.1039/C5RA27080D

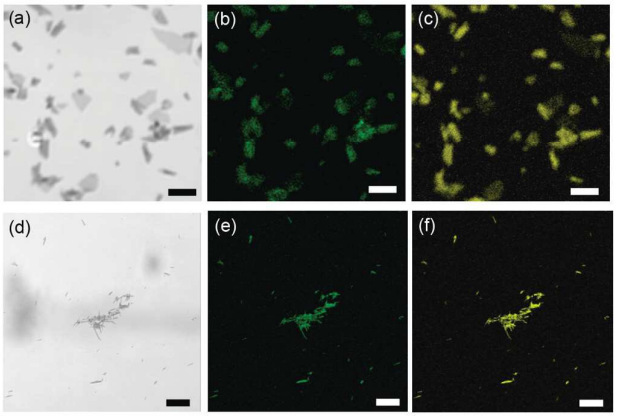

Fig. 6 Bright field, confocal, and two-photon microscopic images of nanosheets (a, b, and c, respectively) and nanoscrolls (d-f). Confocal and two-photon microscopy images were obtained with laser excitation at 488 and 800 nm, correspondingly (scale bar: 2 µm).

The results indicate that the presence of JCNs can significantly reduce the laser power effective for cancer therapy due to the dynamic photothermal effects of the JCNs. As the probability of a TP event is favourably relied on the light intensity, conditions can be regulated such that this only occurs appreciably in the focal plane of light (red square) provided from a pulsed laser, leading to highly precise spatial targeting. Accordingly, in the example given, it is possible to target a single blood vessel, without extensive collateral damage or toxic adverse effects. Moreover, the cells within the irradiation spot were completely dead after 2 h, showing very few adjacent cells nearby the region were affected due to diffusion of the released drug molecules (Fig. 7c).

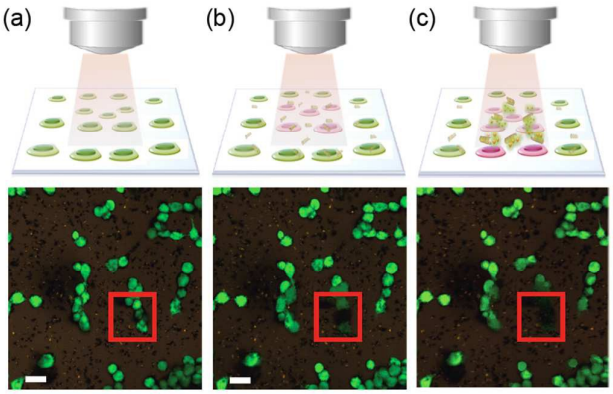

Fig. 7 Effects of JCNs loaded with Dox on the two-photon photothermal therapy of HeLa cells (a-c). The cells were incubated with JCNs for 12 h and calcein acetoxymethyl ester was used to label live cells: (a) with JCNs, before therapy, (b) with JCNs, after 30 min two-photon laser irradiation at 0.1 mW, (c) Dox release after 2 h at 37°C to mimic the release under physiological conditions after the TP-treatment. Scale bar: 30 µm.

Further study on optimizing such TP-induced targeting and releasing behavior of drug-loaded JCNs in clinical settings will be required for addressing *in vivo* efficacy of the formulation.

4. Conclusion

We developed heterogeneously organized hybrid organic-inorganic JCNs in responsive to the triple stimuli, e.g. pH, drug, and NIR light. The use of these JCNs as an insoluble drug delivery vehicle and an effective photosensitizer for PTA or TP-PTA *in vitro* were demonstrated on HeLa cell treatment under single- or two-photon irradiation, by employing MTT assay (indirect method), and fluorescence microscopy (direct method). In particular, the scrolled geometry of JCNs, incorporating PCL moieties inside the wall was turned to our advantage to minimize the drug release, before targeting the desirable sites. Triggered release could be achieved upon heating, which leads to a phase change of the crystalline PCL domains into the amorphous state: Reversely resemble like natural spore containers, which respond as rolled structures when hydrated, while unrolling by tension and torsion arise with the dehydration). Moreover, internal heating could be also advantageously generated, thanks to the presence of JCN interior and the application of NIR irradiation, thereby allowing a triggered drug (spore) release through remote NIR activation. The combined result of the synergistic contribution of phototherapy and chemotherapy, in guidance of imaging, and the stable complex formulation make JCNs as attractive agent for targeted cancer treatment, cancer-cell ablation, smart molecular probe, or drug delivery vehicle, in a minimally-invasive fashion.

Acknowledgements

Authors gratefully acknowledge Dr. T. Sasaki and Dr. V. Singh for their technical assistance with TEM and AFM imaging, respectively.

References

1 a) Y. Bar-Cohen, *Biomimetics: Biologically Inspired Technologies*, CRC Press, Boca Raton, FL 2005, pp. 1-552; b) M. Lattuada, T. A. Hatton, *Nano Today*, 2011, **6**, 286; c) I. Burgert, P. Fratzl, *Philos. Transact. R. Soc. Math. Phys. Eng. Sci.* 2009, **367**, 1541; d) S. Armon, E. Efrati, R. Kupferman, E. Sharon, *Science* 2011, **333**, 1726; e) R. Elbaum, L. Zaltzman, I. Burgert, P. Fratzl, *Science* 2007, **316**, 884; f) P. Fratzl, R. Elbaum, I. Burgert, *Faraday Discuss*. 2008, **139**, 275; g) E. Reyssat, L. Mahadevan, *J. R. Soc. Interface* 2009, **6**, 951; h) X. Noblin, N. O. Rojas, J. Westbrook, C. Llorens, M. Argentina, J. Dumais, *Science* 2012, **335**, 1322.

2 a) A. Walther, A. H. E. Müller, *Chem. Rev.* 2013, **113**, 5194; b) F. Liang, K. Shen, X. Qu, C. Zhang, Q. Wang, J. Li, J. Liu, Z. Yang, *Angew. Chem. Int. Ed.* 2011, **50**, 2379; c) X. Ji, Q. Zhang, F. Liang, Q. Chen, X. Qu, C. Zhang, Q. Wang, J. Li, X. Song, Z. Yang, *Chem. Commun.* 2014, **50**, 5706; d) H. Yang, F. Liang, X. Wang, Y. Chen, C. Zhang, Q. Wang, X. Qu, J. Li, D. Wu, and Z. Yang, *Macromolecules*, 2013, **46**, 2754; e) Z. Zhao, F. Liang, G. Zhang, X. Ji, Q. Wang, X. Qu, X. Song, Z. Yang, *Macromolecules*, 2015, **48**, 3598.

View Article Online
DOI: 10.1039/C5RA27080D

3 J.-H. Kim, M. Bohra, C. Cassidy, V. Singh, M. Sowwan, *ACS Appl. Mater. Inter.* 2014, **6**, 13339.

4 F. Zhang, Z. Jia, M. F. Srinivasan, *Langmuir* 2005, **21**, 3389.

5 a) R. L. Reis, N. M. Neves, J. F. Mano, M. E. Gomes, A. P. Marques, H. S. Azevedo, *Natural-Based Polymers for Biomedical Applications* CRC Press, Boca Raton, FL 2008, pp. 129-154; b) K. Yao, J. Li, F. Yao, Y. Yin, *Chitosan-Based Hydrogels: Functions and Applications* CRC Press, Boca Raton, FL 2012, pp. 235-338; c) M. L. Jayme, D. E. Dunstan, M. L. Gee, *Food hydrocolloids* 1999, ***13***, 459.

6 a) X. Huang, P. K. Jain, I. H. El-Sayed, M. A. El-Sayed, *Nanomedicine* 2007, **2**, 681; b) T. Niidome, Y. Akiyama, M. Yamagata, T. Kawano, T. Mori, Y. Niidome, Y. Katayama, *J. Biomater. Sci. Polym.* 2009, **20**, 1203; c) A. M. Alkilany, L. B. Thompson, S. P. Boulos, P. N. Sisco, C. J. Murphy, *Adv. Drug Deliver. Rev.* 2012, **64**, 190.

7 L. Nie, M. Chen, X. Sun, P. Rong, N. Zheng, X. Chen, *Nanoscale* 2014, **6**,1271-6.

8 Y. N. Zhong, C. Yang, L. Cheng, F. H. Meng, Z. Y. Zhong, Z. Liu, *Biomacromolecules* 2013, **14**, 2411.

9 a) D. Mondal, M. Griffith, S. S. Venkatraman, *Int. J. Polym. Mater.* 2016, ***65***, 255; b) H. Deng, J. Liu, X. Zhao, Y. Zhang, J. Liu, S. Xu, L. Deng, A. Dong, J. Zhang, *Biomacromolecules* 2014, ***15***, 4281.

10 J. Olson, S. Dominguez-Medina, A. Hoggard, L.-Y. Wang, W.-S. Chang, S. Link, *Chem. Soc. Rev.* 2015, **44**, 40.